Characterization, fouling, and performance of synthesized chitosan–glycerol membranes in bacterial removal from municipal wastewater

Elon I. Cadogan[a], Ching-Hwa Lee[a], Srinivasa R. Popuri[b,*], Hang-Yi Lin[a]

[a]Department of Environmental Engineering, Da-Yeh University, No. 168, University Rd., Dacun, Changhua 51591, Taiwan, ROC, emails: elon.cadogan@gmail.com (E.I. Cadogan), chl@mail.dyu.edu.tw (C.-H. Lee), qq0985779726@gmail.com (H.-Y. Lin)
[b]Department of Biological and Chemical Sciences, The University of the West Indies, Cave Hill Campus 11000, Barbados, Tel. +1 246 417 4340; Fax: +1 246 417 4325; email: popurishrinu@gmail.com

ABSTRACT

The inherent hydrophilic nature of chitosan has gained significant attention with respect to its application in water treatment processes. This study was aimed to synthesize chitosan–glycerol (CSG) membranes for microfiltration (MF) applications in wastewater treatment via the solution casting and solvent evaporation technique. CSG membranes were prepared in the ratios 2:1, 3:1, and 4:1 and were cross-linked with phosphoric acid in the presence of ethanol. The synthesized membranes were characterized by tensile strength, swelling, Fourier transform infrared spectroscopy-attenuated total reflectance and Scanning electron microscopy studies to investigate their structural properties. The porosifier glycerol had a great influence on the tensile strength and elongation than the cross-linker. The pore size distribution of the membranes ranged from 28.1 to 51.6 Å with BET surface areas of 13.8–23.8 m^2 g^{-1}. Water permeation studies were conducted using a cross-flow MF module in batch analyses. The results indicated that 2:1 CSG membranes effectively removed over 95% of bacteria notably, *Escherichia coli* from wastewater. Various blocking mechanisms were investigated and are discussed in detail utilizing various fouling models such as standard, intermediate, complete, and cake formation, of which the cake formation model had the highest correlation coefficient of these models.

Keywords: Chitosan; Glycerol; Membrane; Water treatment; Microfiltration; Pore blocking

1. Introduction

The increasing demand for water and limited water resources has led to the reclamation and reuse of municipal wastewater. Various pressure-driven membrane based water treatment processes include microfiltration (MF), ultrafiltration (UF), nanofiltration (NF), and reverse osmosis (RO) are introduced for the treatment of wastewater. MF has low maintenance and operation costs and is easily operated in comparison to other high-pressure methods such as NF and RO. The physical and chemical characteristics of the membrane material are important for these pressure-driven processes. The pore sizes of MF membranes are generally in the range of 0.1–10 μm, which is effective for the removal of bacterial species in wastewater. However, a major drawback encountered with these processes is the membrane fouling phenomenon [1].

*Corresponding author.

Membrane fouling involves the adsorption of foulants, through physical and/or chemical processes, present in the feed liquid being transported across the membrane [2]. There has been various membrane fouling processes proposed that include surface fouling, inter-membrane fouling, membrane pore fouling, and cake formation fouling. These have been attributed but not limited to proteins, oil, natural organic matter, and bacteria that are often found in high concentration in untreated municipal wastewater effluents and the removal substances can contribute to pollution control [3–6]. These fouling mechanisms subsequently lead to the development of various types of fouling resistance models such as the complete blocking, intermediate blocking, standard blocking, and cake formation models and are used to evaluate the most probable fouling mechanisms occurring for a specific pressure-driven filtration process. To investigate the fouling state of the membranes, modified Hermia models based on the type of membrane setup, that is cross-flow, dead end etc., have been studied to elucidate the various fouling mechanisms [6].

Bacterial reduction is one of the important parameters for the reuse of municipal wastewater. The main species found in municipal wastewater streams are the fecal bacteria *Escherichia coli* (*E. coli*), *Enterococci*, and fecal coliforms [7,8]. *E. coli,* among other bacterial species, is a commonly used conventional bacterial indicator for wastewater quality and standards [9]. MF treatment is one of the economical wastewater treatment processes that can eliminate such kind of bacterial species and are deemed as a preferred treatment method [10].

The derived biopolymer chitosan (CS) has received considerable attention as a multifunctional polymer due to its relatively versatile chemical compatibility, nontoxicity, hydrophilicity, and biodegradability [11–13]. Its acetylated counterpart chitin is the second most common biopolymer in nature. CS has been used as a membrane in many industrial processes such as MF, UF, NF, RO, gas separation, dialysis, and pervaporation [14–16]. The diverse nature of CS biopolymer film has allowed it to also be used in antibacterial, food biotechnology, pharmaceutical, and medical applications. CS membrane is used in water treatment applications in the form of composite, polyelectrolyte, and blending with another polymer [17]. In filtration processes, the solute and membrane interactions are important in order to study the fouling and performance of the membrane. Glycerol has been used as a plasticizer or porosifier for most film applications in food packaging materials [18–20].

In this study, the isolated chitosan from crab shells is used to synthesize MF membranes with glycerol as a porosifier for municipal wastewater treatment. The membranes are prepared in the ratio of chitosan to glycerol as 2:1, 3:1, and 4:1 and cross-linked with phosphoric acid. The main objective of this study is to evaluate the effect of fouling mechanism and effect of membrane composition on MF performance in bacterial removal of the synthesized chitosan–glycerol (CSG) membranes. In order to study the physiochemical characteristics, the membranes are extensively characterized by tensile strength, elongation, static swelling, Fourier transform infrared spectroscopy-attenuated total reflectance (FTIR-ATR), and scanning electron microscopy (SEM) studies. The various blocking models such as complete, incomplete, standard, and cake formation are studied to evaluate the fouling mechanism of the CSG membranes in the MF process.

2. Experimental

2.1. Materials

Acetic acid glacial and glycerol were purchased from Merck, Germany. Eosin Methylene Blue Agar Power No. 04-8322232 was obtained from Himedia Co. Other chemical reagents such as phosphoric acid were of analytical grade with a purity of 99% and purchased from Merck Chemical Co. Wastewater used in this study was collected from municipal wastewater storage wells near Da-Yeh University, Taiwan. Deionized water was used wherever it was necessary in this study.

2.2. Municipal wastewater characteristics

To determine the initial wastewater characteristics of the water samples, conventional chemical oxygen demand (COD), biological oxygen demand 5-d test (BOD$_5$), total organic carbon, Total solids (TS) and pH measurements were carried out according to the method described in the Standard Methods for the analysis of water and wastewaters [21].

2.3. Chitosan extraction from crab shells

According to Muzzarelli et al., CS can be extracted from crab shells through processes of demineralization, deproteinization, deacetylation, and decoloration [22]. Many large-scale processes, mainly for material synthesis, utilizing large quantities of chitosan take advantage of the added economic benefit of preparing chitosan from available crustacean waste. Industries, such as the food, environmental, and biomedical industries, have proven this process to be economically feasible [23,24]. The waste *Ranina ranina* crab

shells were washed several times with deionized water and dried for 24 h. The dried crab shells were ground to 50 mesh. In the demineralization step, 10 g of this powder and 150 mL of 1 N HCl was transferred into a 250-mL round-bottom flask and subjected to refluxation for 30 min at 60°C. Then the solid was separated from the liquid by vacuum filtration and the dried solid was washed with deionized water until the pH reached neutral. The obtained demineralization solid was deproteinized by stirring the above solid with 3% NaOH solution with a 1:10 (w/v) solid/liquid ratio for 30 min at 80°C. During deproteination, the solution changed to dark orange color. The obtained liquid mixture was filtered and the solid was washed in the same manner mentioned above and then dried for 48 h at room temperature. The resulting chitin material appeared as a faint yellow solid and was subjected to deacetylation with 45% NaOH in a 1:10 (w/v) solid/liquid ratio and treated for 1 h on a hot plate at 80°C. The anionic hydroxyl group in the NaOH provided a negative charge after dissociation in solution that initiated deacetylation by attacking the electron deficient carbonyl group on chitin. The samples were washed again with NaOH, filtered, and sun dried for 6 h. Thus, the CS obtained was a creamy white solid powder.

2.4. Membrane preparation

CSG membranes were prepared by the dissolution of chitosan and glycerol in the appropriate weights, as shown in Table 1. A sufficient quantity of CS was dissolved in 1% acetic acid solution and stirred at 80°C and the required quantity of glycerol was also added to the CS solution in order to get the composition ratio of CSG 2:1, 3:1, and 4:1 and the reaction mixture was stirred for a further 2 h to form a homogenous solution. The membrane forming solutions were allowed to form a membrane via the solution-casting solvent evaporation method on a leveled clean glass surface. The solvent was allowed to evaporate at ambient conditions for 48 h. After evaporation of the solvent, the membranes were removed from the glass plate

Table 1
Chitosan and glycerol weights for membrane solutions obtained at 80°C and 200 rpm stirring velocity

Membrane	Chitosan weight (g)	Glycerol weight (g)	Chitosan: Glycerol ratio
A	3.33	1.67	2:1
B	3.75	1.25	3:1
C	4	1	4:1

and dried. Two percent phosphoric acid in 40% ethanol was used as the cross-linking solution to cross-link the prepared CSG membranes. The resulting CSG membranes were immersed in the cross-linking bath for 4 h. After cross-linking, the membranes were removed and washed repeatedly with water until neutral pH was obtained, followed by drying. The dried membranes were stored in desiccators at room temperature for further use.

2.5. Membrane characterization

2.5.1. Stress–strain mechanical properties

The investigated mechanical properties determine whether the fabricated membranes would be appropriate for MF processes. The tensile strength and elongation percentage of the membrane were measured using a Young Gi Son Co. Ltd, model 2025 Tensile Strength Tester. The equations below were used to calculate the tensile strength and elongation:

$$\sigma = \frac{L}{A} \tag{1}$$

$$\in = \frac{L_f}{L_i} \times 100 \tag{2}$$

where σ is the stress (Nmm^{-2}), L is the load (N), A is the area (mm^2), $\in$ is the strain (%), L_i is the initial membrane length (mm), and L_f is the final membrane length (mm).

2.5.2. Static swelling

Membrane swelling was studied using a conventional gravimetric method. The membrane (0.5 g) was immersed in a 100-mL beaker of double-distilled water. The weights of the swollen membranes were recorded after 24 h after superficially removing surface water with filter paper. The static swelling percentage was calculated using Eq. (3) below:

$$\%S_W = \frac{W_s - W_d}{W_d} \times 100 \tag{3}$$

where W_d is the weight of the dry membrane and W_s is the weight of the swollen membrane.

2.5.3. Fourier transform infrared spectroscopy

The FTIR spectra of all three CSG membranes were obtained using Perkin-Elmer 1600 Spectrophotometer

over the wavenumber range 4,000–500 cm^{-1} with 20 scan at 4 cm^{-1} resolutions. The CSG membranes were analyzed directly using attenuated total reflectance (ATR).

2.5.4. Scanning electron microscope studies

SEM studies were carried out using a multi-function scanning electron microscope 219 (JSM-6400) at the required magnification. The samples were dried at a temperature of 105°C and deposited on a brass holder under vacuum pressure. The voltage acceleration used was 15 kV with the secondary electron image as the detector.

2.5.5. Brunauer–Emmett–Teller, Barrett–Joyner–Halenda, and T-plot micropore analysis

To investigate the porous nature of the synthesized CSG membranes, Porous Materials Incorporated, USA, analyzed the pore size, surface area, porosity etc. Brunauer–Emmett–Teller (BET), Barrett–Joyner–Halenda (BJH) and T-Plot micropore analysis were utilized to derive the various isotherms. Nitrogen gas was used as the adsorbate at a testing temperature of −195°C in the relative pressure range of 0.02–0.1, after the samples were conditioned by outgassing to 20 microns vacuum at 60°C.

2.6. MF filtration experiments

MF performance of the synthesized CSG membranes were conducted on a laboratory constructed MF setup shown in Fig. 1 below. The membrane module used in this setup was cross-flow filtration module with an effective membrane area of 38 cm^2 and

operated with the inlet pressure of 40 psi. The feed solution of municipal wastewater was pumped to the cross-flow filtration membrane module and the permeate flux and flow velocity were measured and recorded using a digital recorder. MF experiments were carried out at a temperature of 25°C. The water fluxes through the membranes were measured as a function of time.

2.7. Quantification of bacteria

The method adopted for the quantification of bacteria was from the American Public Health Association for Standard Methods for Examination of Water and Wastewater [21]. The agar plate method was used to determine the number of *E. coli* colony-forming units present in the wastewater samples. Eosin methylene blue agar used in this study was prepared by adding 18 g of EMB in 1 L of deionized water at 80°C for 1 h. The solution was allowed to cool to 60°C and then poured into Petri dishes, then sterilized before use. For viable counts, 10-fold dilutions were conducted to reduce the *E. coli* colonies from too numerous to count (TNTC) to a range between 30 and 300 CFU per plate. Subsequently, the following calculation was used to determine the number of cells per mL.

$$\text{Number of cells per mL} = \text{CFU} \times \text{dilution factor} \quad (4)$$

After a suitable dilution factor was determined, bacterial suspensions of the wastewater samples were incubated for 24 and 48 h at 35°C and the colonies were counted. The statistic microbial monitoring data is represented by the geometric mean summarized by the equation below:
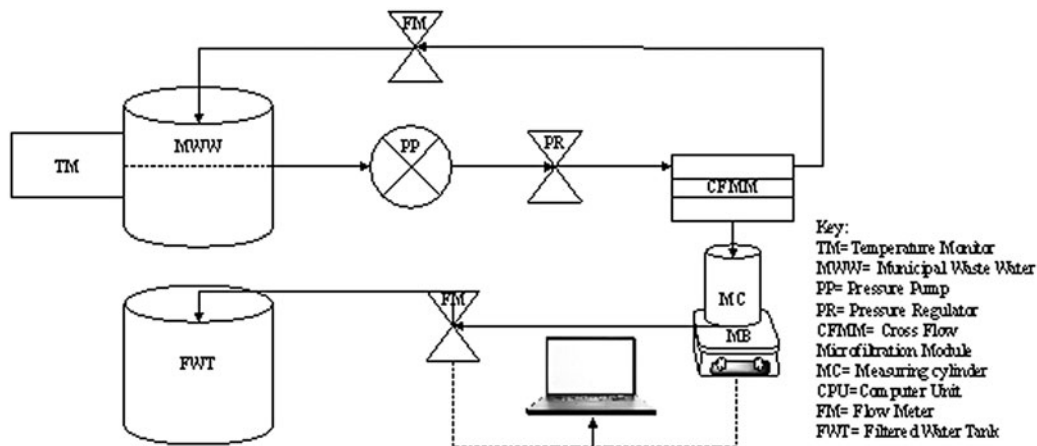

Fig. 1. Laboratory constructed cross-flow MF setup.

$$\overline{x_g} = \sqrt[n]{(x_1)(x_2)(x_3)\dots(x_n)} \qquad (5)$$

where $\overline{x_g}$ is the geometric mean of total samples, x is the average CFU for each set and n is the total number of sample sets.

For an evaluation of the antibacterial activity, the following equation was used to measure the percent inhibition of bacteria:

$$\% \text{ inhibition} = [(CFU_i - CFU_f)/CFU_i] \times 100 \qquad (6)$$

where CFU_i is the initial concentration of *E. coli* and CFU_f is the finial concentration of *E. coli*.

3. Results and discussions

3.1. Municipal wastewater characterization

In support of the assessment of the application of the fouling models, the wastewater samples were characterized based on COD, BOD$_5$, TOC, TS, and pH parameters to categorize the wastewater strength. These characterizations revealed that the wastewater COD, BOD$_5$, TOC, and TS concentrations were 286.7, 412, 208.4, and 842 mg L^{-1} with a pH 7.9. Based on these investigations, the wastewater strength was categorized as medium to high strength due to the relatively high BOD$_5$ contaminants in comparison to the relatively moderate concentration of COD contaminants [25].

3.2. Membrane cross-linking

CSG membranes were synthesized and due to hydrophilic nature of CS the flat membranes were cross-linked with phosphoric acid. The amino groups of the CS reacted with the phosphate groups of phosphoric acid and formed a strong ionic bond between the polymer and the cross-linking agent [16,26,27]. Fig. 2 represents the cross-linking reaction of the CSG membranes with the phosphoric acid.

3.3. Membrane characterizations

3.3.1. Stress–strain mechanical properties

For the comparison of the strength of the synthesized flat cross-linked CSG membranes, the
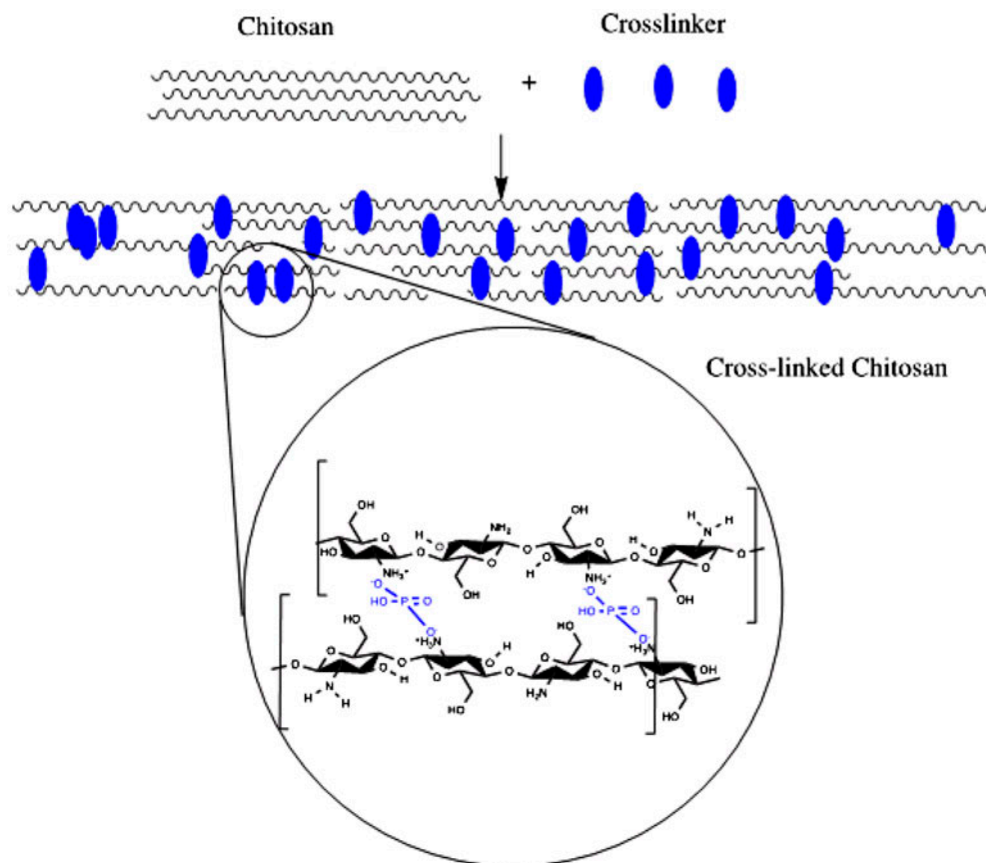

Fig. 2. Cross-linking scheme of chitosan in the cross-linking solution of phosphoric acid and ethanol.
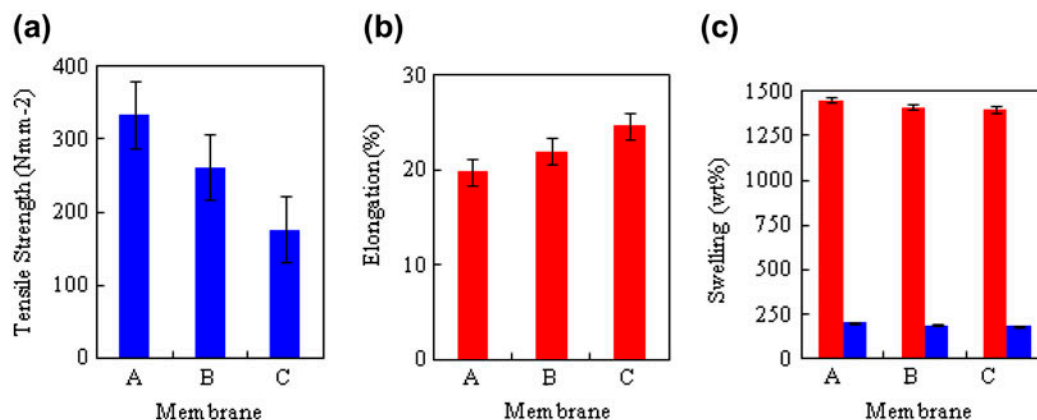
Fig. 3. (a) CSG membrane tensile strengths, (b) membrane elongations, and (c) membrane static swelling.

membranes were subjected to tensile strength and elongation studies presented in Fig. 3(a) and (b). From the results, it was observed that the tensile strength of the membranes increased (elongation decreases) as the CS content of the CSG membranes increased. It was observed that the CSG ratios had a significant effect at the 95% confidence level through ANOVA tests of the tensile strengths and elongation values, resulting in standard deviations of 78.5 and 2.42 with absolute deviations of 52.3 and 1.61, respectively.

The CSG membrane C exhibited the highest elastic properties, followed by CSG membrane B and then A. This has been attributed to the high glycerol content in membrane C relatively compared with membrane B and A in the CS matrix. The glycerol in the CS matrix occupies pores in the membrane and prevents the collapsing of the membrane or pores as the solvent evaporates [28]. The glycerol also functioned as a plasticizer, thus increasing the stretching ability or elasticity of the membranes. Hence, CSG membrane C had higher elongation compared with CSG membrane A, which had the higher tensile strength due to their chemical composition.

3.3.2. Static swelling

Static swelling studies were conducted for the CSG membranes before and after cross-linking with phosphoric acid and these results are represented in Fig. 3(c). After cross-linking, all the membranes had a dramatic decrease in water uptake capacity. The swelling of CSG membranes had a decrease in the magnitude of 7.07, 7.39, and 7.59 for membranes A, B, and C, respectively, which accounted for a minimum sevenfold reduction in water uptake capacity for all membranes. ANOVA tests at the 95% confidence level

showed that these swelling values were significantly different with standard deviations of 26.8 and 10.69 with absolute deviations of 17.3 and 7 for non-cross-linked and cross-linked CSG membranes. This water uptake capacity has been attributed to the reduction in the hydrophilic nature of chitosan due to the polymer chain being cross-linked by the phosphoric acid, thus decreasing the availability of amine groups for participation in hydrogen bonding [26]. Additionally, CS polymeric groups after cross-linking created cross-linked structures in the membrane that results in the entanglement of the polymer chains that reduced the absorption of water molecules. However, there was no significant change observed in swelling among the three CSG membranes before and after cross-linking. The average percent swelling of the CSG membranes before and after cross-linking was 1,419 and 193%, respectively.

3.3.3. FTIR analysis

FTIR studies were conducted for all three cross-linked CSG membranes shown in Fig. 4. In the analysis of the spectrum, the broad band seen at 3,450 cm^{-1} belongs to −OH stretching groups of the CSG membranes. From the figure, it was observed that as the content of glycerol in the membranes increased, the broadness of this band also increased, however two different stretching modes have been assigned to −OH stretching (hydrogen bonded), −NH stretching in NH$_2$. −OH stretching was attributed to the intramolecular and/or intermolecular bonding from both chitosan and glycerol contributions in the polymer network. Since the broadness of the peak is due to hydrogen bonding, the increases in absorbance of the wavelength between 3,200 and 3,600 cm^{-1} have
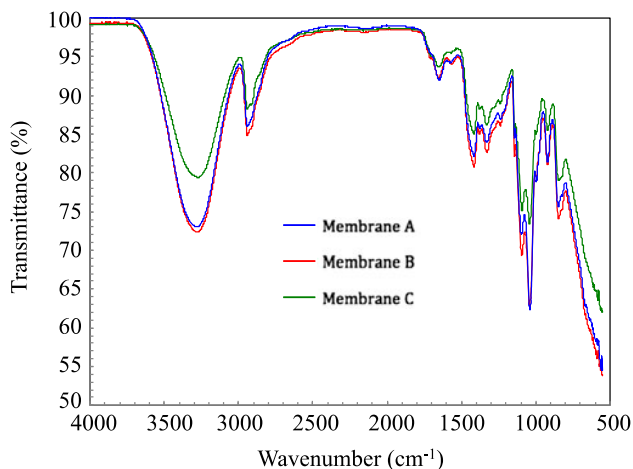
Fig. 4. FTIR spectra of the CSG membranes.

been subsequently correlated to the increased presence of glycerol in the membranes. There are three hydroxyl groups present per molecule of glycerol, which can therefore give rise to an intricate network. The partial negative charge of the nitrogen in NH_2 can

attract electron-deficient bonded hydrogens nearby. The peak around the wavelength of $2,900 \text{ cm}^{-1}$ was assigned to $-CH$ stretching of CS and glycerol. As the glycerol content in the CSG membrane increased the frequency increased. The peak at approximately $1,420 \text{ cm}^{-1}$ has been assigned to the presence of NH_3^+ deformation and the peak at around $1,150 \text{ cm}^{-1}$ has been assigned to P=O stretching and $-OH$ deformation arising in cross-linking.

3.3.4. SEM analysis

SEM analysis was carried out to determine the surface morphology of the cross-linked CSG membrane *A* before and after cross-flow filtration experiments and is shown in Fig. 5 (membranes *B* and *C* are not shown here). From the SEM images, it was clearly noticed that the deposition of material from the wastewater on the surface of the membrane, indicated by the gray particles, after MF experiments. The initial SEM image of Membrane *A* is presented in Fig. 5(a) and the SEM image after MF experiments is shown in Fig. 5(b). Fig. 5(c) and (d) shows the lateral view of the
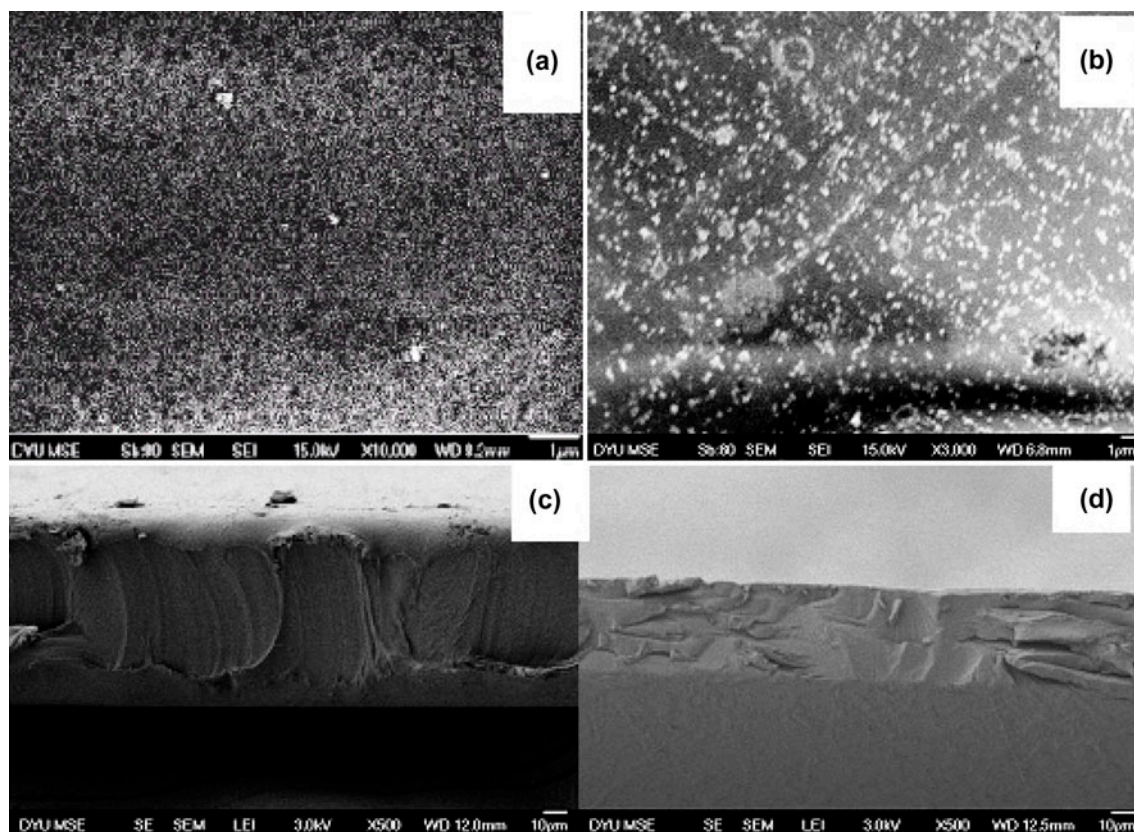

Fig. 5. Membrane surface morphology (surface and cross-section) of Membrane *A* before cross-flow MF (a and c) and Membrane *A* after cross-flow MF (b and d).

membranes; initially the membrane had a thickness of about 65 μm, however after MFC operation and drying, the membrane thickness was reduced to about 40 μm, due to the possible compressing of the membrane when placed into the MFC module and subjected to the MFC operating pressure. The change in surface morphology of the membrane was attributed to the deposition of particles from the wastewater.

3.3.5. Brunauer–Emmett–Teller, Barrett–Joyner–Halenda, and T-plot micropore analysis

The porous characteristics of the synthesized membranes were determined by BET, BJH, and T-Plot micropore analysis, and their results are summarized in Table 2. Based on BET analysis, the membranes were observed to have specific surface areas of 13.8, 23.8, and 19.2 $m^2 g^{-1}$ for membranes A, B, and C, respectively, which surface areas corresponded well to the pore sizes of 60.7, 42.3, and 47.9 Å, respectively. The relation could be seen that as the pore size increased, the specific surface area decreased. These BET values were in good agreement with the BJH analysis, although the trade-off relation was of a lower magnitude. The BJH pore size distributions were 51.6 and 30.23 (Membrane A), 44.81 and 28.1 (Membrane B), and 45.7 and 28.5 (Membrane C) based on pore volume and surface area, respectively. The pore volumes of the membranes were 0.021, 0.025, and 0.023 Å for membranes A, B, and C, respectively, which corresponded well with their BJH porosity. These porosities can be speculated to play an integral part in the effective restriction of transmembrane movement [29]. The T-Plot micropore analysis indicated that the porous surface areas, porosity, and internal and external

surface areas also followed a similar trend to the BET and BJH analysis.

3.4. Permeate flux and membrane resistance in cross-flow MF

The permeate flux behaviors of all three cross-linked CSG membranes were investigated and the results were shown in Fig. 6(a). The flow rate was calculated using Darcy's Law that applied the relation between the transmembrane pressure (TMP), total resistance R_t, and the dynamic viscosity (μ) as shown below in Eq. (7).

$$ J = \frac{\text{TMP}}{R_t \mu} \tag{7} $$

The initial flux for the cross-linked CSG membranes A, B, and C were 148, 160, and 184 $Lm^{-2} h^{-1}$, respectively. These initial values decreased as cross-flow MF proceeded until a quasi-steady-state flux of 89, 91, and 96 $Lm^{-2} h^{-1}$ were attained after about 8 min for the cross-linked CSG membranes A, B, and C, respectively. This was attributed to the accumulation of foulants, which were present in the wastewater. The total resistances of the three cross-linked CSG membranes were investigated and the results were presented in Fig. 6(b). The total resistance was calculated as the sum of the resistance of the clean membrane R_m and the resistance of the fouled membrane R_f. The initial resistances of the cross-linked CSG membranes A, B, and C were 7.96, 7.36, and $6.43 \times 10^8 m^{-1}$, respectively. As time evolved, there were significant increases in the resistances of the

Table 2
BET, BJH, and T-Plot micropore analysis

| Membrane | Brunauer–Emmett–Teller analysis | | Barrett–Joyner–Halenda analysis | | | | T-plot micropore analysis | | |
	S_{ext} ($m^2 g^{-1}$)	$\bar{d}$ (Å)	V_{pore} ($cm^3 g^{-1}$)	$P_{s,d}$ (g^{-1})	$\bar{d}_{vol}$ (Å)	$\bar{d}_{s,ext}$ (Å)	S_{int} ($m^2 g^{-1}$)	ε	S_{int}/S_{ext}
A	13.822	60.722	0.021	0.0104	51.63		30.23		20.385
	0.0442	1.474							
B	23.835	42.298	0,025	0.0124	44.814		28.034		25.807
	0.0525	1.08							
C	19.172	47.850	0.023	0.0151	45.685		28.492		22.44
	0.048	1.17							

Notes: S_{ext}: BET specific surface area; $\bar{d}$: BET mean pore size; V_{pore}: BJH pore size distribution; $P_{s,d}$: BJH porosity (based on skeletal density (0.500 g/cc); $\bar{d}_{vol}$: BJH mean pore diameter (based on pore volume); $\bar{d}_{s,ext}$: BJH mean pore diameter (based on surface area); S_{int}: porous surface area; ε: porosity.
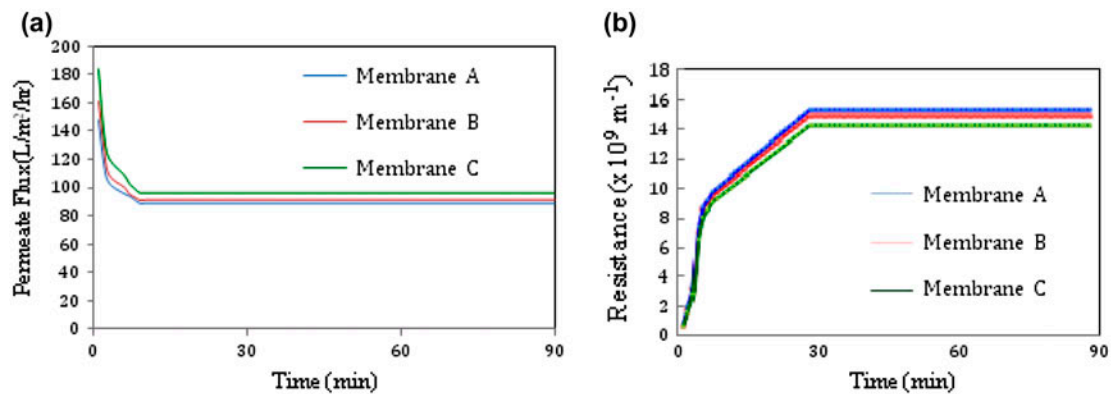
Fig. 6. Permeate flux (a) and membrane resistance (b) during cross-flow MF for cross-linked CSG membranes A, B, and C.

CSG membranes, which after about 26 min reached a steady state and the resistances were 15.4, 15, and 14.3×10^9 m^{-1} for CSG membranes A, B, and C, respectively. Similarly to the decrease in permeate flux observed, the accumulation of foulants on or in the CSG membrane matrixes caused membrane pore blocking, thus increasing the resistance of all three cross-linked CSG membranes.

3.5. Fouling mechanisms and blocking laws

The particles present in wastewater migrated toward the membrane and accumulated on the membrane surface that resulted in the blocking of the pores or cake formation, thus increasing the resistance during MF operation. Pore blocking models conveniently interpret the fouling mechanism in dead-end and cross-flow MF of bacteria before it passes through the extracellular polymer substance [30]. The following four pore blocking mechanisms were used to describe the fouling phenomenon of polymer membranes by bacteria, colloidal particles and proteins: (1) complete pore blocking, (2) intermediate pore blocking, (3) standard pore blocking, and (4) cake formation blocking, which are illustrated in Fig. 7. These models were developed for dead-end filtration and are based on constant pressure filtration laws. At constant pressure, the dependence of time on filtrate volume is expressed as:

$$\frac{d^2 t}{dV^2} = k \left(\frac{dt}{dV} \right)^n \tag{8}$$

where k and n are constants depends on membrane characteristics, operational conditions. The exponent n is the blocking index equal to 2 for complete blocking, 1.5 for standard blocking, 1 for intermediate blocking, and 0 for cake formation.
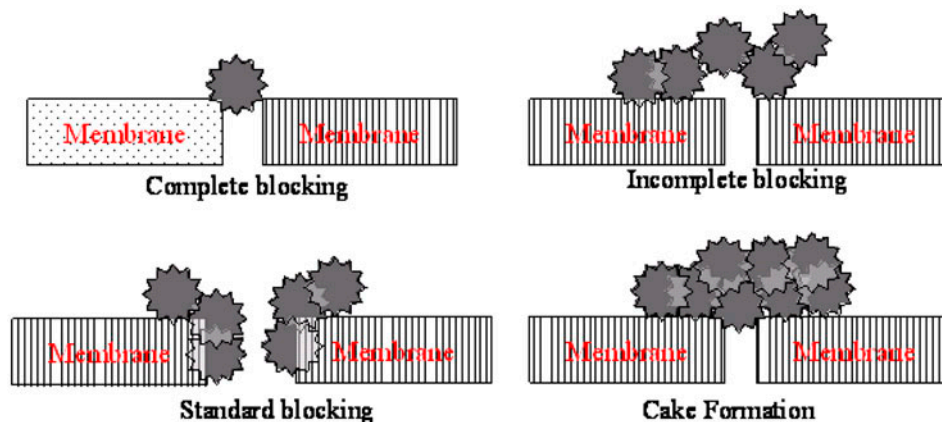

Fig. 7. Illustration of fouling mechanisms for complete blocking, incomplete blocking, standard blocking and cake formation.

3.5.1. Complete blocking model

According to the complete blocking model (CBM), each particle attached to the CSG membrane surface, contributing to pore blocking that eventually blocked the effective membrane entrance area completely without overlapping [31,32]. For the constant pressure filtration process, the relation between time, (t), permeate flux, (J), and initial permeate flux (J_0), was expressed as Eq. (9).

$$K_b V = Q_0 (1 - e^{-kbt}) \qquad (9)$$

The linear expression of the above equation can be written as:

$$\ln(J^{-1}) = \ln(J_0^{-1}) - k_b t \qquad (10)$$

where k_b indicates the cake blocking mechanism constant.

In this model, a linear relationship was established between J and time (t) shown in Fig. 8(a). The main advantage of using linear expression is that it allows for facile identification of individual fouling mechanisms based on an easily determinable correlation coefficient. The newly established resistance was inversely proportional to the fraction of free pores since blocked pores were now considered impermeable. The parameter fit values of CBMs were shown in Table 3. It was seen that CSG membrane C had the best correlation coefficient for this model, which indicates that the membrane with highest pore blocking was CSG membrane C.

3.5.2. Intermediate blocking model

The intermediate blocking model (IBM) postulates that particles settle on the surface of the CSG membranes and other particles settle on top of previously settled particles already. In this model, the blocking arises when the solute particle size is similar to the membrane pore size. During this process, the blocked pores on the surface of the CSG membranes are assumed to be proportional to the reduced filtrate volume. However, the IBM is only concerned with the blocking of pores at the CSG membrane surfaces. For constant pressure filtrations processes, the relationship between time, (t), and permeate flux, (J^{-1}), was expressed as Eq. (11) [32].
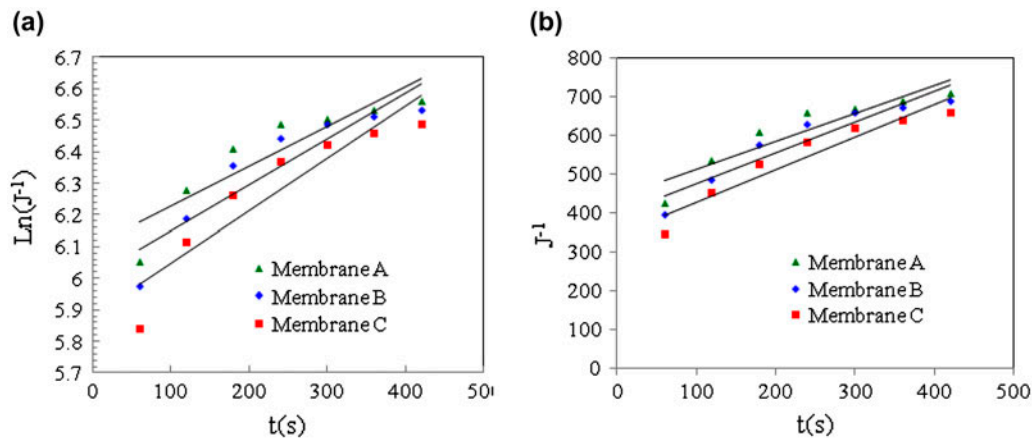

Fig. 8. Linear plots of fouling resistance models by (a) complete blocking (b) intermediate blocking.

Table 3
Complete and IBMs fit parameters and correlation coefficients for CSG membranes operated in cross-flow MF

Model	Membrane	Linear fit parameter values	R^2 value
Complete	A	$k_b = 0.0013 \ s^{-1}$	0.82
	B	$k_b = 0.0015 \ s^{-1}$	0.85
	C	$k_b = 0.0015 \ s^{-1}$	0.86
Intermediate	A	$k_i = 0.721 \ s^{-1}$	0.86
	B	$k_i = 0.794 \ s^{-1}$	0.89
	C	$k_i = 0.836 \ s^{-1}$	0.91

$$J^{-1} = J_0^{-1} - k_i t \qquad (11)$$

The parameter fit values of IBMs were shown in Table 3. It was seen that CSG membrane C had the better correlation coefficient for this model, which indicates that the membrane with highest pore blocking was CSG membrane C and this was previously indicated by the CBM.

3.5.3. Standard blocking model

The standard blocking model (SBM), as shown in Fig. 9(a), assumes that the membrane pores were perfect transmembrane cylindrical pores. As solid matter, smaller than the pore diameter, enters the pores, particles became affixed to the inner walls of the pores and hence decreased the pore volume. This decrease in size as solid matter accumulated on the pores of the wall causes a decrease in pore radius, which is expressed as resistance. The resistance was calculated as a function of volume. The decrease in filtrate volume for all CSG membranes was attributed to be proportional to the permeate volume. For constant pressure filtration this blocking model was dependent extensively on the volumetric flow rate:

$$J^{-1/2} = J_0^{-1/2} - k_s t \qquad (12)$$

where J_0 is the initial flux and k_s is the standard blocking constant. The fit parameter values and correlation coefficient of all the CSG membranes further indicated

that the highest internal pore blocking of the walls occurred in CSG membrane C.

3.5.4. Cake formation blocking model

In cake formation blocking model (CFM), the solute molecular size is greater than the membrane pore size which do not pass through the pores results the formation of cake layer on the membrane surface [28]. The linearized form is expressed as:

$$J^{-2} = J_0^{-2} - k_c t \qquad (13)$$

The parameters of liner fit of CFM were shown in Table 4. It was seen that CSG membrane C had the best correlation coefficient 0.96 compared to other two CSG membranes A and B for this model. This indicates that the membrane C undergo cake formation that blocks the pores of the surface and decrease the flux rate with time.

Table 4
Standard and cake blocking models Fit parameters and correlation coefficients for CsG membranes operated in cross-flow MF

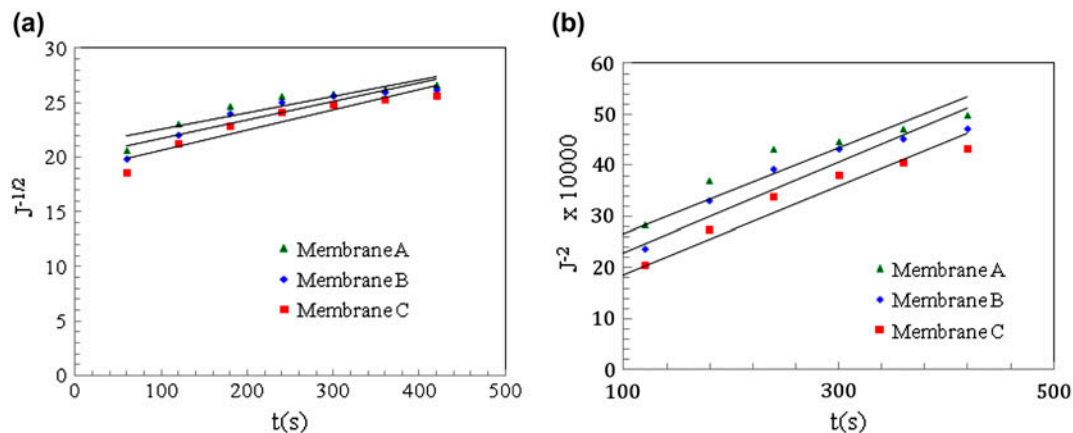| Model	Membrane	Fit parameter values	R^2 value
Standard	A	$k_s = 0.0151$ s^{-1}	0.83
	B	$k_s = 0.017$ s^{-1}	0.87
	C	$k_s = 0.0186$ s^{-1}	0.88
Cake	A	$k_c = 837.58$ s^{-1}	0.90
	B	$k_c = 881.72$ s^{-1}	0.92
	C	$k_c = 863.42$ s^{-1}	0.96

Fig. 9. Linear plots of fouling resistance models by (a) standard blocking and (b) cake formation.

Among the four Hermia's models tested to interpret the fouling phenomenon occurring in the MF experiments with wastewater, cake formation blocking and IBMs are fitting better for experimental data obtained. The regression coefficient values in Table 4 indicate that the membranes are blocked by first intermediate blocking and followed by cake formation due to bigger size of the solute particles than the CSG membranes pore size.

3.6. Bacterial removal efficiency

MF performance of the CSG membranes was assessed on the removal of bacteria from wastewater and the results were depicted in Fig. 10. Generally, a membrane pore size is less than 1 μm would reject the bacterial species from passing through the membrane due to physical barrier. The results in Fig. 10 indicated that CSG membrane *A* had the highest bacterial removal efficiency of about 95% compared to CSG membranes *B* and *C*, which were 93 and 92%, respectively. All membranes had an average pore size of less than 1 μm, however, membrane *A* had the smallest pore size and thus the differences in bacterial removal efficiency can been attributed to the differences in pore size. The pore size result of CSG membranes measured by SEM studies also provided good evidence with the high bacterial removal efficiency of membrane *A*. Since membrane *A* had a high tensile strength that resulted in the low flux value compared to the other two membranes, therefore high percentage of bacterial removal is quite obvious with the existence of trade off relationship. Hence the results revealed that a low percentage of glycerol in polymer matrix was efficient in removing the bacteria from wastewater. 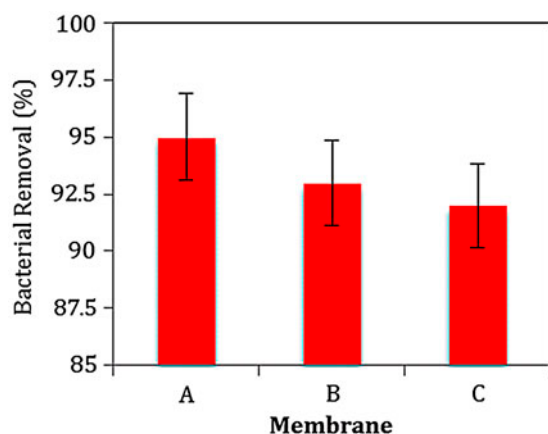Although membrane *A* performance is higher than membranes *B* and *C*, all the membranes were proven effective (greater than 90%) in removal of bacteria from wastewater.

4. Conclusions

(1) The simple polyol compound, glycerol, was used as porosifier to regulate the pore size of chitosan membranes within the range of 28.1–51.6 Å.
(2) FTIR studies identified the characteristic –OH and amine I and II groups of chitosan and the P=O group of phosphoric acid. SEM studies revealed that membrane compression occurred and the thickness decreased from 65 to 40 μm subsequent to the filtration process.
(3) The various fouling models studied such as complete blocking, intermediate blocking, standard blocking, and cake formation were used to investigate the fouling state present, and cake formation was deduced to be the most dominant form of fouling present due to the higher correlation coefficients of all the CSG membranes.
(4) The results indicated that 2:1 CSG membranes effectively removed over 95% of bacteria notably, *E. coli* from wastewater.

Fig. 10. Bacterial removal efficiencies of CSG membranes *A*, *B*, and *C*.

References

[1] R.W. Baker, Membrane Technology and Applications, (second ed.), J. Wiley, Chichester, New York, NY (2004).
[2] Y.J. Zhao, K.F. Wu, Z.J. Wang, L. Zhao, S.S. Li, Fouling and cleaning of membrane, J. Environ. Sci. 12 (2000) 241–251.
[3] D. Rana, T. Matsuura, Surface modifications for antifouling membranes, Chem. Rev. 110 (2010) 2448–2471.
[4] G. Harms, A.C. Layton, H.M. Dionisi, I.R. Gregory, V.M. Garrett, S.A. Hawkins, K.G. Robinson, G.S. Sayler, Real-time PCR quantification of nitrifying bacteria in a municipal wastewater treatment plant, Environ. Sci. Technol. 37 (2003) 343–351.
[5] K. Zhang, K. Farahbakhsh, Removal of native coliphages and coliform bacteria from municipal wastewater by various wastewater treatment processes: Implications to water reuse, Water Res. 41(12) (2007) 2816–2824.
[6] M. Abbasi, A. Taheri, Modeling of permeation flux decline during oily wastewaters treatment by MF-PAC hybrid process using mullite ceramic membranes, Indian J. Chem. Technol. 21 (2014) 49–55.
[7] X. Bonjoch, E. Balleste, A.R. Blanch, Multiplex PCR with 16S rRNA gene-targeted primers of *Bifidobacterium* spp. to identify sources of fecal pollution, Appl. Environ. Microbiol. 70 (2004) 3171–3175.

[8] Y. Nebra, X. Bonjoch, A.R. Blanch, Use of *Bifidobacterium dentium* as an indicator of the origin of fecal water pollution, Appl. Environ. Microbiol. 69(5) (2003) 2651–2656.

[9] J. Jofre, Chapter 11 Indicators of waterborne enteric viruses, in: Perspectives in Medical Virology 17 (2007) 227–249.

[10] S.S. Madaeni, A. Khorasani, M. Asgharpour, S.A. Ghoreshi, Removal of mixtures of viruses using micro-filtration membrane, Desalin. Water Treat. 51(22–24) (2013) 4313–4322.

[11] S.I. Nishimura, O. Kohgo, K. Kurita, Chemospecific manipulations of a rigid polysaccharide: Syntheses of novel chitosan derivatives with excellent solubility in common organic solvents by regioselective chemical modifications, Macromolecules 24 (1991) 4745–4748.

[12] H. Sashiwa, Y. Makimura, R. Roy, Y. Shigemasa, Chemical modification of chitosan: Preparation of chitosan–sialic acid branched polysaccharide hybrids, Chem. Commun. 11 (2000) 909–910.

[13] N.R. Sudarshan, D.G. Hoover, D. Knorr, Antibacterial action of chitosan, Food Biotechnol. 6 (1992) 257–272.

[14] B. Krajewska, Diffusion of metal ions through gel chitosan membranes, React. Funct. Polym. 47 (2001) 37–47.

[15] S. Jana, A. Saikia, M.K. Purkait, K. Mohanty, Chitosan based ceramic ultrafiltration membrane: Preparation, characterization and application to remove Hg(II) and As(III) using polymer enhanced ultrafiltration, Chem. Eng. J. 170 (2011) 209–219.

[16] S.R. Popuri, S. Sridhar, A. Krishnaiah, M. Yen Wey, Pervaporation separation of ethylene glycol/water mixtures by using cross-linked chitosan membranes, Ind. Eng. Chem. Res. 46 (2007) 2155.

[17] D.A. Musale, A. Kumar, G. Pleizier, Formation and characterization of poly(acrylonitrile)/Chitosan composite ultrafiltration membranes, J. Membr. Sci. 154 (1999) 163–173.

[18] K.V. Harish Prashanth, R.N. Tharanathan, Chitin/chitosan: Modifications and their unlimited application potential—An overview, Trends in Food Sci. Technol. 18 (2007) 117–131.

[19] J. Bajdik, M. Marciello, C. Caramella, A. Domján, K. Süvegh, T. Marek, K. Pintye-Hódi Evaluation of surface and microstructure of differently plasticized chitosan films. J. Pharm. Biomed. Anal. 49 (2009) 655–659.

[20] R.B. Hawrylko, US PATENT 5198170 Method for exclusion of powered PVC compounds (1993) 1–18.

[21] American Public Health Association (APHA), Standard Methods for the Analysis of Water and Wastewater, seventeenth ed., Washington DC, NY, USA, 1989.

[22] R.A.A. Muzzarelli, C. Jeuniaux, G.W. Gooday, Chitin in nature and technology, Plenum Press, (1986) Science.

[23] Z. Rahimi, A.A. Zinatizadeh, S. Zinadini, Preparation and characterization of a high antibiofouling ultrafiltration PES membrane using OCMCS -Fe$_3$O$_4$ for application in MBR treating wastewater, J. Appl. Res. Water Wastewater 1 (2014) 13–18.

[24] P.K. Dutta, J. Dutta, V.S. Tripathi, Chitin and Chitosan: Chemistry, properties and applications, J. Sci. Ind. Res. 63 (2004) 20–31.

[25] Metcalf and Eddy Inc, 2003, Metcalf and Eddy Inc, Metcalf and Eddy: Wastewater Engineering: Treatment and Reuse, McGraw-Hill Companies Inc, London, 2003.

[26] Y. Wan, K.A.M. Creeber, B. Peppley, V.T. Bui, Synthesis, characterization and ionic conductive properties of phosphorylated chitosan membranes, Macromol. Chem. Phys. 204 (2004) 850–858.

[27] S. Charuchinda, K. Srikulkit, T. Mowattane, Co-application of sodium polyphosphate and chitosan to improve flameretardancy of cotton fabric, J. Sci. Res. 30(1) (2005) 97–107.

[28] P.D. Unger, R.P. Rohrbach, US PATENT 5525710A, Highly porous chitosan bodies, (1996) 1–14.

[29] Y. Xin, M.W. Bligh, A.S. Kinsela, Y. Wang, T.D. David Waite, Calcium-mediated polysaccharide gel formation and breakage: Impact on membrane foulant hydraulic properties, J. Membr. Sci. 475 (2015) 395–405.

[30] J. Hermia, Constant pressure blocking filtration laws: Application to power-law nonNewtonian fluids, Trans. Insti. Chem. Eng. 60 (1982) 183.

[31] K.J. Hwang, T.T. Lin, Effect of morphology of polymeric membrane on the performance of cross-flow microfiltration, J. Membr. Sci. 199 (2002) 41–52.

[32] M.C.V. Vela, S.A. Álvarez Blanco, J.L. García, E. Bergantiños Rodríguez, Analysis of membrane pore blocking models adapted to crossflow ultrafiltration in the ultrafiltration of PEG, Chem. Eng. J. 149 (2009) 232–241.